

Percolative Superconductivity in $\text{Mg}_{1-x}\text{B}_2$

P. A. Sharma,¹ N. Hur,^{1,2} Y. Horibe,^{1,2} C. H. Chen,² B. G. Kim,¹ S. Guha,¹ Marta Z. Cieplak,^{1,3} and S-W. Cheong^{1,2}

¹*Department of Physics & Astronomy, Rutgers University, Piscataway, New Jersey 08854*

²*Bell Laboratories, Lucent Technologies, Murray Hill, New Jersey 07974*

³*Institute of Physics, Polish Academy of Sciences, 02668 Warsaw, Poland*

(Received 7 August 2001; published 27 September 2002)

Our results from various transport experiments on $\text{Mg}_{1-x}\text{B}_2$ indicate a surprising effect associated with the presence of a Mg deficiency in MgB_2 : the phase separation between Mg-vacancy rich and Mg-vacancy poor phases. The Mg-vacancy poor phase is superconducting, but the insulating nature of the Mg-vacancy rich phase probably originates from the Anderson (disorder-induced) localization of itinerant carriers. Furthermore, electron diffraction measurements indicate that within vacancy-rich regions these defects tend to order with intriguing patterns. This *electronic* phase separation in $\text{Mg}_{1-x}\text{B}_2$ shows similar, but also distinct characteristics compared with that observed in $\text{La}_2\text{CuO}_{4+\delta}$.

DOI: 10.1103/PhysRevLett.89.167003

PACS numbers: 74.80.Bj, 61.72.Dd, 74.62.Bf, 74.62.Dh

The phenomenon of electronic phase separation can be characterized as the insolubility of two or more different phases with substantially different electronic character. The occurrence of this effect is well known to underlie the extraordinary electronic and magnetic properties of complex materials. The most notable examples include the magnetoresistive manganites and the high- T_C superconductor $\text{La}_2\text{CuO}_{4+\delta}$ system [1,2]. Remarkably, we have observed electronic phase separation in the recently discovered superconductor MgB_2 , while attempting to study the effect of Mg nonstoichiometry on this compound. This effect is substantiated by intriguing electrical and thermal transport properties as well as a detailed electron microscopy study.

Since the discovery of superconductivity in MgB_2 [3], researchers have been plagued by a variety of problems directly related to its synthesis. While the superconducting transition appears to be rather robust, the magnitude and temperature (T) dependence of the normal state resistivity (ρ) shows considerable variation with preparation conditions. For instance, T_C has been observed to vary from about 35–42 K, and $\rho(T_C)$ and $\rho(300\text{ K})/\rho(T_C)$ can vary from 0.5–20 $\mu\Omega\text{ cm}$ and 2–25, respectively, for carefully prepared single phase MgB_2 (thin films, bulk polycrystals, single crystals). The presence of the three most common impurity phases: MgO, MgB_4 , and nonreacted Mg or boron has partly explained this behavior [4]. However, no in-depth study of Mg vacancy on transport properties has been performed.

In this Letter, we report a variety of transport measurements and a detailed electron microscopy investigation of $\text{Mg}_{1-x}\text{B}_2$ for $0 \leq x \leq 0.15$. Our results are consistent with the phase separation between Mg-vacancy rich and Mg-vacancy poor regions in this material. The relative amounts of these two phases vary with the total amount of Mg vacancy. Furthermore, the electronic nature of the two phases is drastically different. The Mg-vacancy poor phase is a superconducting metal, and the Mg-vacancy rich phase is insulating. Interestingly, these vacancies

were seen to order, but only partially. This particular observation allows a direct, phenomenological comparison with the high- T_C system $\text{La}_2\text{CuO}_{4+\delta}$, in which electronic phase separation has been exhaustively studied.

$\text{Mg}_{1-x}\text{B}_2$ polycrystalline samples with $0 \leq x \leq 0.15$ were prepared by solid-state reaction methods under high pressure. Great care was taken to ensure a systematic variation of Mg deficiency, keeping the amounts of other impurity phases negligible or constant. Starting materials were Mg powder (Alfa Aesar; 99.8%) and submicrometer-size amorphous B powder (Aldrich Chemical; 99.995%). We employed a two-step method for sample synthesis, in order to maximize chemical homogeneity [5–7].

All these materials showed almost identical x-ray diffraction patterns, but their transport properties were drastically different. Each x-ray pattern was consistent with single phase MgB_2 , with little change in the lattice parameters within our resolution ($a \approx 3.085 \pm 0.005 \text{ \AA}$, $c \approx 3.522 \pm 0.005 \text{ \AA}$). There was no indication of the MgB_4 phase and nonreacted crystalline Mg or B, but each specimen was found to contain a small, roughly constant amount of MgO. The potentially significant presence of amorphous, nonreacted B (undetected by x-ray diffraction) was also ruled out with a careful transmission electron microscopy (TEM) and also polarized optical microscope investigations. Contrary to the x-ray diffraction results, the behavior of ρ showed a pronounced variation as shown in Fig. 1(a). Among about two dozen samples synthesized with the above methods, we will discuss only seven representative specimens for clarity. Each has been labeled with a roman numeral (I)–(VII) indicating a separate preparation process, ordered according to the magnitude of ρ . Amazingly, the magnitude of ρ , in the entire temperature range, changes dramatically with Mg vacancy, close to 8 orders of magnitude (at $T \approx 300 \text{ K}$) in total. Note that the most insulating specimen (VII) corresponds to $x \approx 0.15$ and the most metallic specimen (I) corresponds to $x \approx 0$. The normal state and superconducting properties of (I) are

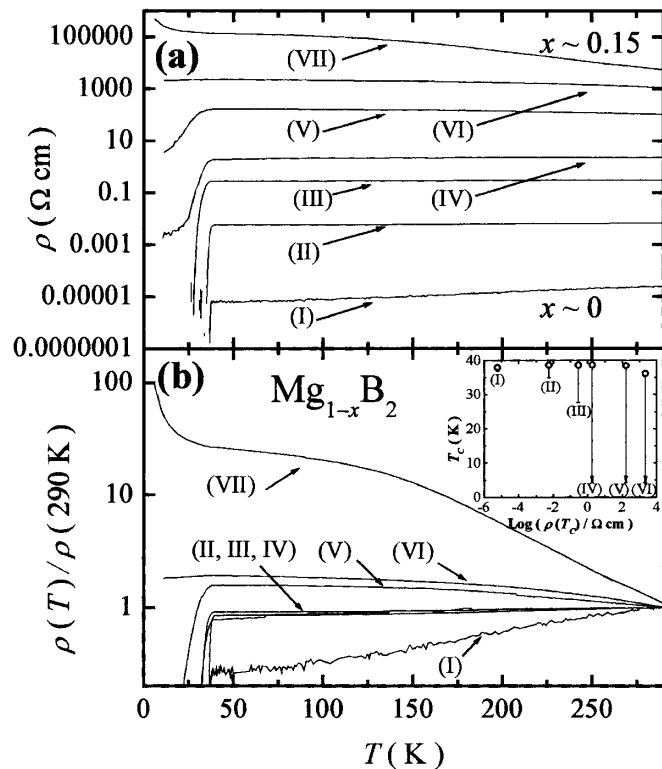


FIG. 1. (a) Resistivity of $\text{Mg}_{1-x}\text{B}_2$ as a function of temperature, $\rho(T)$, for $0 \leq x \leq 0.15$. Roman numerals (I)–(VII) indicate increasing values for x . (b) Normalized resistivity, $\rho(T)/\rho(290 \text{ K})$, of $\text{Mg}_{1-x}\text{B}_2$ for $0 \leq x \leq 0.15$. Roman numerals correspond to those given in (a). Inset: T_C vs $\log(\rho(T_C))$ of $\text{Mg}_{1-x}\text{B}_2$. Solid circles indicate the onset T_C . Solid lines specify the transition width. Arrows show that no superconductivity was observed down to 4.2 K. Amazingly, the resistivity increases by close to 8 orders of magnitude for the range of x we have studied. Note that the metallic behavior of $\rho(T)$ for very resistive specimens demonstrates the percolative nature of electrical conduction.

comparable to the best specimens reported in the literature [$\rho(T_C) \approx 6 \mu\Omega \text{ cm}$, transition width $\approx 1 \text{ K}$]. Interestingly, even the more resistive samples (II)–(VII) became as metallic as (I) (both in magnitude and T dependence) after annealing in Mg vapor, indicating that any Mg deficiency is easily replenished. Therefore, we infer that this drastic change in resistivity is solely due to the presence of Mg vacancies. While the change in the magnitude of ρ was roughly systematic with the attempted increase of x for $\text{Mg}_{1-x}\text{B}_2$, this correlation in the two dozen samples we investigated was not exact. This is probably due to the nonreproducibility of Mg evaporation during each step of the synthesis method. Nonetheless, we expect an approximately one-to-one correspondence between $\rho(T)$ and Mg deficiency.

Perhaps the most striking feature of ρ is that the T dependence remains metalliclike (up to sample V) even though the magnitude becomes enormously large (up to $\sim 100 \Omega \text{ cm}$), much larger than the Mott metallic limit ($\rho_{\text{Mott}} \approx 2 \text{ m}\Omega \text{ cm}$), as x increases. This behavior is emphasized in Fig. 1(b), which shows $\rho(T)/\rho(290 \text{ K})$. Only

the most resistive samples (VI, VII) begin to show signs of insulating T dependence. This trend is indicative of percolative conduction through metallic regions separated by insulating regions [2]. Examining the influence of Mg vacancies on the superconductivity of each sample further supports this conclusion. As shown in the inset of Fig. 1(b), the onset superconducting transition temperature, T_C (determined using a 2%–3% onset condition), remains nearly constant while the transition width systematically broadens with the increase of $\rho(T_C)$. The onset of superconductivity completely disappears for only the most insulating specimen (VII). The suppression of superconductivity in this particular way is very similar to that seen in granular systems with clustered regions of a superconductor such as Sn deposited on an insulating substrate [8]. In the cases of homogeneously disordered (on the length scale of a lattice parameter) superconductors, it is well established experimentally that T_C steadily decreases as $\rho(T_C)$ increases. Thus, the behavior of the resistivity strongly suggests that the system $\text{Mg}_{1-x}\text{B}_2$ is a mixture of a superconducting-metallic phase and (an) insulating phase(s), and that the relative volume of these phases change with the overall Mg-vacancy concentration.

To understand the electronic nature of this insulating phase of Mg-deficient MgB_2 , we have measured the thermal conductivity, $\kappa(T)$, and thermoelectric power, $S(T)$, for this series of specimens as shown in Fig. 2. First, all but the most metallic sample (I) ($x \approx 0$) have a negligibly small normal state electronic contribution to κ according to the Wiedemann-Franz law, and so the phonon contribution dominates. For clarity, we have shown only $\kappa(T)$ for (I, II, VII), but the remaining specimens are similar in behavior to (VII). Thus, the resistive samples are near some minimal thermal conductivity, which can indicate a large amount of disorder. Disordered crystals with an increasing amount of lattice disorder show an analogous lowering of the lattice thermal conductivity to some minimum value [9]. Measurements of S on selected samples, as displayed in Fig. 2(b), show the magnitude increasing systematically with increasing Mg vacancy. We were unable to measure S in the entire T range for the most resistive samples due to the high contact resistance. Noticeably, the magnitude of S ($T \approx 300 \text{ K}$) for the most resistive specimens is uncharacteristically small ($\sim 30 \mu\text{V/K}$) compared to other materials with a comparable ρ ($\geq 10^3 \Omega \text{ cm}$) [10]. In fact, this incommensurability between ρ and S is an indication of disorder-induced (Anderson) localization [11]. The T dependence of the thermopower also supports this explanation, in that the magnitude decreases with decreasing T . This is a crucial test that can distinguish thermally activated hopping (one sign of Anderson localization) from a true energy gap, for which case S increases with decreasing T [10]. It is noteworthy that from the behavior of $\rho(T)$ the percolation threshold for the conduction through the metallic region seems to be between (IV)

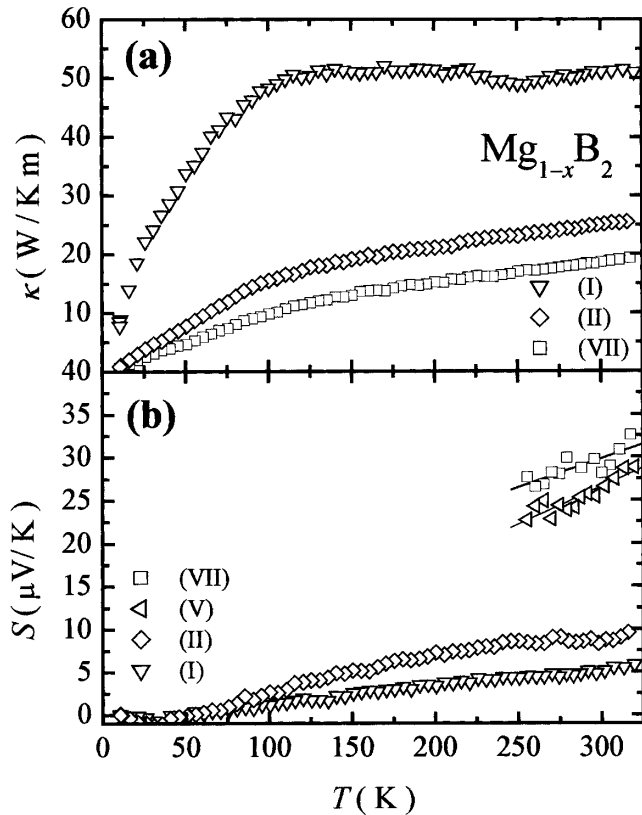


FIG. 2. (a) Thermal conductivity of $\text{Mg}_{1-x}\text{B}_2$ as a function of temperature, $\kappa(T)$. Only specimens (I), (II), and (VII) are shown for clarity. (b) Thermoelectric power of $\text{Mg}_{1-x}\text{B}_2$ as a function of temperature, $S(T)$. Only specimens (I), (II), (V), and (VII) are shown for clarity. The small magnitudes of both κ and S for the most resistive samples exemplify an Anderson (disorder-induced) insulating phase.

and (V). Since the percolation threshold for the three-dimensional mixtures of a metal and an insulator is at $\sim 15\%$ volume fraction of the metallic phase, it is likely that sample (VII) is predominantly made up of the insulating phase. In this way, $\kappa(T)$ and $S(T)$ possibly indicate that the insulating nature of the Mg-vacancy rich phase originates from the Anderson localization of itinerant carriers.

Our TEM results provide further evidence for this phase coexistence. Our studies were carried out at room temperature in a JEOL-2000FX transmission electron microscope equipped with a 14-bit charge-coupled array detector. Most electron diffraction patterns (incident electron beam parallel to the [001] zone axis) showed a simple hexagonal pattern consistent with the known lattice parameters. However, a few distinctive patterns, classified as rotated \sqrt{N} -type superlattices, were occasionally seen due to the presence of superstructures in which the size of the supercell is \sqrt{N} ($N = \text{integers}$) times larger than the unit cell. In $\text{Mg}_{1-x}\text{B}_2$ samples, we have identified several diffraction patterns corresponding to the $\sqrt{7}$, $\sqrt{13}$, $\sqrt{19}$, $\sqrt{28}$, and $\sqrt{31}$ type superlattices. The rotated $\sqrt{19}$ and $\sqrt{13}$ type superlattices, shown in Figs. 3(a) and 3(b), were seen

most frequently. Each superlattice is rotated from the fundamental hexagonal lattice by an angle of 23.4° (for $\sqrt{19}$) and 13.9° (for $\sqrt{13}$). The reflection spots were indexed in a consistent manner using the hexagonal notation. Interestingly, the $\sqrt{13}$ superlattice is basically the same as the patterns observed in charge-density wave (CDW) materials (e.g., 1T-TaSe₂) [12]. The presence of

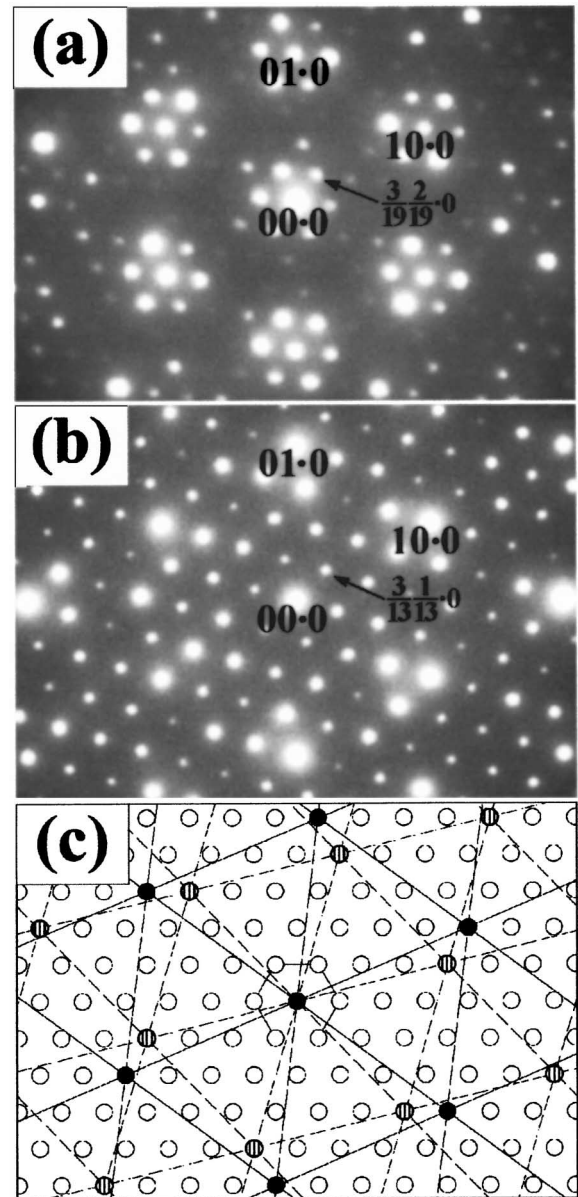


FIG. 3. (a) Electron diffraction patterns showing the $\sqrt{19}$ superlattice observed for specimen (III). (b) Electron diffraction patterns showing the $\sqrt{13}$ superlattice observed for specimen (IV). Both patterns were obtained at room temperature with the incident electron beam parallel to the [001] zone axes. Reflection spots are indexed in the hexagonal notation. (c) Schematic figure of the vacancy ordering observed in (a) and (b) on the Mg sublattice. Closed circles and solid lines denote the $\sqrt{19}$ superlattice. Striped circles and dashed lines denote the $\sqrt{13}$ superlattice. The small hexagonal lattice corresponds to the unit cell of Mg atoms.

the \sqrt{N} superlattice is consistent with simple vacancy ordering in the Mg sublattice. Figure 3(c) shows how vacancy ordering occurs in a single Mg layer for the $\sqrt{19}$ and $\sqrt{13}$ superlattices. The closed circles and the solid lines denote the $\sqrt{19}$ superlattice; the striped circles and the dashed lines denote the $\sqrt{13}$ superlattice. One can easily devise other \sqrt{N} vacancy ordering superlattice cells following the same approach. Note that concentrations of the Mg vacancy in the $\sqrt{19}$ and $\sqrt{13}$ superlattices are $\sim 5.26\%$ and $\sim 7.69\%$, respectively. Several distinct \sqrt{N} superlattice patterns were observed in a given sample, suggesting that the Mg-vacancy distribution is significantly inhomogeneous. Also, the regions with superlattices are less common compared to regions without superlattices, for example, $\sim 10\%$ in (III) and $\sim 20\%$ in (VII). The disparity of the regions with and without superlattice spots clearly indicates that the $\text{Mg}_{1-x}\text{B}_2$ samples are highly inhomogeneous in terms of vacancy ordering, and that vacancy ordering is only partial. Mg-vacancy-ordered regions likely contain additional, disordered Mg vacancies. We also studied the diffraction patterns along the [100] direction and found no indication of superlattices.

While TEM does not directly probe the Mg-vacancy disordered regions, vacancy ordering was found to occur in samples with metallic T dependence of ρ (e.g., III) as well as highly resistive samples (e.g., VII). This observation is indicative of phase separation into Mg-vacancy poor and Mg-vacancy rich regions, exemplified by the $\text{La}_2\text{CuO}_{4+\delta}$ system, in which oxygen-rich and oxygen-poor regions coexist [13]. In this material, a miscibility gap opens below a characteristic temperature (~ 290 K) between certain critical values of δ . This, in turn, drives the system to phase separate into two critical compositions. The high mobility of the excess oxygen allows ordering to occur readily even below ~ 290 K, but the temperature at which vacancy ordering occurs in the $\text{Mg}_{1-x}\text{B}_2$ system may be quite high, perhaps near the synthesis temperature. The low mobility of the Mg vacancy is most likely the reason for this and should also prevent complete vacancy ordering in $\text{Mg}_{1-x}\text{B}_2$.

The origin of the insulating nature of the Mg-vacancy rich phases is certainly intriguing. There exists a large attractive Coulombic interaction between Mg^{2+} and the boron p_π orbital, which plays a crucial role in producing the different electronic character between graphite and hexagonal boron layers in MgB_2 [14]. Mg vacancies naturally eliminate this interaction, resulting in a large impurity potential. This large impurity potential probably leads to significant disorder effects by disordered Mg vacancies such as the Anderson localization of charge carriers in boron layers. However, a change in carrier concentration due to Mg vacancies can also play an additional role in producing an insulating ground state.

We have reported a surprising change in the transport properties of MgB_2 with the introduction of Mg-vacancy point defects. Interestingly, these vacancies were seen to

order with fascinating patterns. These observations are indicative of phase separation. Furthermore, our findings reveal that the phase separation in $\text{Mg}_{1-x}\text{B}_2$ results in the natural coexistence of two electronically distinct phases: a superconducting metal and an Anderson-type insulator. Whether this effect results from the chemistry of defect clustering or the electronic stability of phase separated systems is still a topic of debate.

We thank J. B. Neaton, A. Perali, G. Kotliar, and E. Abrahams for useful discussions. This work was supported by the National Science Foundation under Grant No. 0103858.

-
- [1] J. Ryder *et al.*, *Physica* (Amsterdam) **173C**, 9 (1991).
 - [2] M. Uehara, S. Mori, C. H. Chen, and S.-W. Cheong, *Nature* (London) **399**, 560 (1999).
 - [3] J. Nagamatsu *et al.*, *Nature* (London) **410**, 63 (2001).
 - [4] C. B. Eom *et al.*, *Nature* (London) **411**, 558 (2001).
 - [5] First, starting materials were lightly mixed and pressed into pellets in a glove box. The pellets were sealed into a Ta tube and fired in a tube furnace at 900°C for 2 h under a mixed gas of 92% Ar + 8% H_2 . Second, the reacted pellets were reground, then sintered in Au capsules under high pressure (up to 15 kbar) at $650\text{--}700^\circ\text{C}$ for 0.5–2 h in a cylinder-piston type apparatus (Ref. [6]). The stoichiometric sample (I) was then annealed in Mg vapor at 900°C for 6 h, after high-pressure sintering.
 - [6] C. U. Jung *et al.*, *Physica* (Amsterdam) **353C**, 162 (2001).
 - [7] From a preliminary electron microprobe analysis, specimens (I, II, IV, and VII) showed chemical compositions of $x \approx 0, 0.08, 0.1, \text{ and } 0.12$, respectively. The spatial resolution was $\sim 1\ \mu\text{m}$, with a compositional uncertainty of $\sim 10\%$. In addition, we have performed qualitative energy dispersive x-ray fluorescence spectroscopy (EDS), with a transmission electron microscope (TEM), on specimen (IV) to examine the homogeneity of chemical composition across the grain boundaries (spatial resolution $\approx 100\ \text{\AA}$, compositional resolution $\approx 10\%$). This careful work indicates that the chemical composition is homogeneous across grain boundaries within our resolution and that there is no spurious phase (such as amorphous boron) at the grain boundaries.
 - [8] J. M. Valles, Jr. and R. C. Dynes, in *Physical Phenomena in Granular Materials*, edited by G. D. Cody, T. H. Geballe, and Ping Sheng (Materials Research Society, Pittsburgh, PA, 1990), p. 375.
 - [9] D. G. Cahill, S. K. Watson, and R. O. Pohl, *Phys. Rev. B* **46**, 6131 (1992).
 - [10] P. M. Chaikin, in *Organic Superconductivity*, edited by V. L. Kresin and W. A. Little (Plenum Press, New York, 1990), p. 101.
 - [11] G. Sherwood, M. A. Howson, and G. J. Morgan, *J. Phys. Condens. Matter* **3**, 9395 (1991).
 - [12] See, e.g., G. Grüner, *Density Waves in Solids* (Addison-Wesley Publishing Company, Reading, MA, 1994).
 - [13] J. D. Jorgensen *et al.*, *Phys. Rev. B* **38**, 11 337 (1988).
 - [14] J. M. An and W. E. Pickett, *Phys. Rev. Lett.* **86**, 4366 (2001).